Research Project 1 - 085851
Technion - Israel Institute of Technology
Faculty of Aerospace Engineering
January 2024

Experimental and numerical investigation of combustion dynamics in a diffusion flame, using hydrogen and nitrogen

Shai Karolinsky Davidovich

Advisor: Associate Prof. Dan Michaels

Contents

List of Figures

Abstract

This research is a continuation of Ojha's et al. study [1], which examined the impact of nitrogen dilution on pollutant emissions in a swirl burner in premixed and non-premixed hydrogen/air combustion as well as methane-hydrogen mixtures. In this research, we investigate the effect of nitrogen dilution on flame dynamics in hydrogen/air combustion using the same swirl burner as Ojha et al [1], in its non-premixed setup. We analyze the flame behavior by capturing OH PLIF measurements and conducting one-dimensional numerical diffusion flame simulations. The different cases examined provided different types of turbulent diffusion flames. Hydrogen produced a flame classified in the wrinkled and stretched flamelets regime, whereas nitrogen-diluted hydrogen produced a flame with a discontinuous front, somewhere along the transition between a perturbed flamelet and a thickened flame. This shows the dilution lowered Da number, and raised Re and Ka number, as the turbulent flows intensified by the augmented momentum and vortices smaller than the reaction zone are presumably responsible for the broken flame front. Further investigation is required for validation.

Introduction

Ojha et al. [1] presented how nitrogen dilution results in a dramatic decrease in NO_x emissions, from 80 ppm to approximately 3 ppm, as seen in Fig. 1. This presents us the opportunity to replace the use of natural gas, which results in approximately 20 ppm NO_x emissions, with hydrogen.

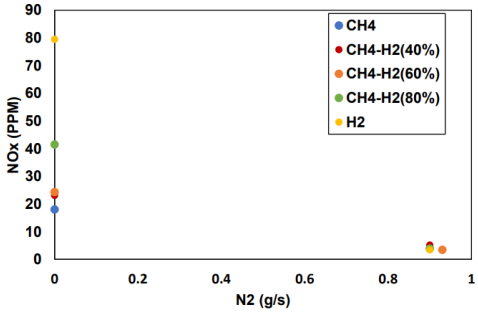

[1]

Figure 1. NO_x emissions level as a function of nitrogen dilution during non-premixed combustion of fuel mixtures, taken from P. Kumar Ojha [1] research

Achieving higher engine performances may often result in increased pollutant emissions of poisonous gasses with major environmental effects, such as nitric oxides NO_x $(NO,\ NO_2)$, and carbon monoxide CO. Consequently, environmental regulations are getting more and more restrictive over the years.

In the set of experiments that will be held, we will observe turbulent diffusion flames. Diffusion flames are controlled by diffusion, directed by the flow, meaning turbulence is a key factor and highly affects the flames' dynamic [2]. The Borghi-Peters [3] diagram describes the different types of turbulent diffusion flames:

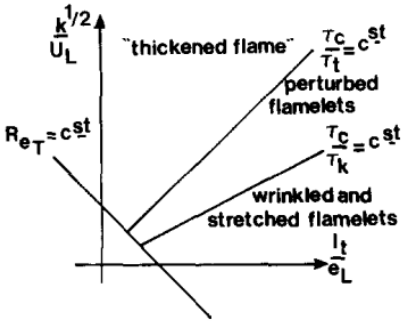

[3]

Figure 2. Types of Turbulent Diffusion Flames

The dimensionless axes are l_t/e_L, $k^{\frac{1}{2}}/U_L$ when k is the turbulence kinetic energy, U_L is the laminar flame velocity, l_t is the integral length scale of the turbulence, and e_L is the laminar flame thickness. The expression of c^{st} represents the transition between two regimes, with a transition region of some thickness.

The area below the curve of $Re_T = c^{st}$ represents the non-turbulent regime, the following will discuss the turbulent regime alone ($Re_T > c^{st}$). The flame can be divided into three different regimes: wrinkled and stretched flamelets, perturbed flamelets, and "thickened flame". The line of τ_c/τ_K represents the local extinction limit. When τ_c/τ_K is smaller than its critical value, the turbulent flow does not locally extinguish the flames, but the flame will appear wrinkled and stretched, which increases the surface area and reaction zones [4]. The wrinkling: A_T/A. The flamelets thickness e_D can be measured as:

$$e_D \propto \sqrt{d \cdot \tau_K} \propto \eta \tag{1}$$

τ_K^{-1} – the mean stretching rate, d – the common diffusion coefficient, η – the Kolmogorov microscale.
In the "perturbed flamelets" regime, above the critical value of τ_c/τ_K, flamelets can locally quench and the structure of the flame becomes more complicated and unsteady. Lastly, for a higher value of τ_c/τ_t ratio, τ_t being the turbulent mixing time scale, we can address the diffusion flame almost as a premixed flame, at the "thickened flame" regime. The chemistry time scale is large compared to the turbulent

mixing time scale, and the turbulent mixing rate is high enough to partially premix the fuel and air, causing the non-premixed flame to appear as a premixed one [4].

The scalar dissipation rate χ (of the mixture number) is defined as the rate at which the fuel concentration dissipates due to the effects of turbulent mixing. In turbulent diffusion flames, the reactants are primarily mixed by the flow, and the scalar dissipation rate is a vital/ helpful parameter in learning about the mixing process.

$$\chi = D\left(\frac{\partial Z}{\partial x_j}\frac{\partial Z}{\partial x_j}\right) \tag{2}$$

$$\chi_{st} = D_f \cdot |\nabla Z_{st}|^2 \tag{3}$$

Also:

$$\nabla Z \approx \frac{1}{l_f} \quad \Longrightarrow \quad \chi_{st} = \frac{D_f}{|l_f|^2} \tag{4}$$

l_f being the flame thickness (the nomenclature differs between the articles, although it was mentioned above as e_D). D_f being the diffusion coefficient. The hydrogen diffusion coefficient in air is approximately $0.8\ [cm^2/s]$ in 300 K.

Damkohler number Da is defined as the ratio between the flow time rate and the chemical time rate:

$$Da = \frac{\tau_f}{\tau_c} \tag{5}$$

In turbulent non-premixed combustion, the flow time scale τ_f can be described as the inverse of the scalar dissipation $\frac{1}{\chi}$ causing the D_a number to appear in the form of [2]:

$$Da = (\tau_c \chi)^{-1} = \frac{{l_f}^2}{D_f \cdot \tau_c} \tag{6}$$

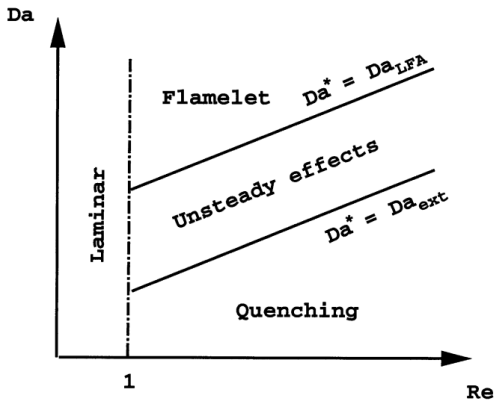

[5]

Figure 3. Schematic of non-premixed turbulent combustion regimes as a function of Da and Re, taken from [5]

The transition between different types of turbulent flames can be classified by the change in Damkohler number. For $Da > Da_{LFA}$, the flow time scale is significantly larger than the chemical time scale, the combustion is fast, and we can consider it close to the infinitely fast chemistry limit [2], which can fit the wrinkled and stretched flamelets regime, where the vortices are larger than the combustion zone. For $Da < Da_{ext}$ the chemistry is slow, the chemical time scale is larger than the flow time scale, vortices are smaller than the combustion zone and stronger strain rates cause local quench. The flame will locally extinguish causing the combustion to occur in a distributed form, at the thickened flame regime. The area stated as unsteady affects $Da_{ext} < Da < Da_{LFA}$ refers to the perturbed flamelet regime in Fig. 2.

When discussing premixed flames, it is common to address the Karlovitz number instead of the Damkohler number. $Da = 1/Ka$, in the sense of studying the interaction of the flame with the smallest turbulence scale (Kolmogorov scale $\tau_\eta = \frac{\eta}{u_\eta}$) we can define the Karlovitz number as:

$$Ka = \frac{\tau_{flame}}{\tau_\eta} = \frac{l_f^2}{\eta^2} \tag{7}$$

Where τ_f is the flame time scale and is defined in this case as l_f/U_L.

$$Ka > 1 \quad \Longrightarrow \quad l_f > \eta \tag{8}$$

$Ka > 1$ is the limit where the eddies become smaller than the combustion zone $l_f > \eta$ and local quenching begins, resulting in a broken reaction zone.

Overview of The Research

1. **Experimental study in a non-premixed combustor**:

   Four different cases are examined using planar laser-induced fluorescence (PLIF) in a non-premixed swirl combustor. The oxidizer is air in all cases $(21\%\ H_2,\ 78\%\ N_2, and\ 1\%\ AR)$, while fuel mixtures differ for each experiment, keeping the same air flow rates and power outputs of 19.5 kw:

   (a.) 100% hydrogen, $\phi = 0.5$.

   (b.) Nitrogen diluted hydrogen: 76% H_2, 24% N_2, $\phi = 0.5$.

   (c.) Nitrogen diluted hydrogen: 64% H_2 36% N_2, $\phi = 0.5$.

   (d.) 100% methane, $\phi = 0.6$.

2. **Numerical study of diffusion flames**:

   Solving a one-dimensional opposed-flow diffusion flame case using the Cantera [6] "CounterFlowDiffusionFlame" function to present OH, NO, and NO_2 molar fractions, and the mixture fractions of each case. Including Scalar dissipation rates and axial velocity gradients calculations, showing the stretch rates the flame is experiencing until extinction. The extinction points were computed using the scaling rules derived by Fiala and Sattelmayer [7].

Experimental Setup

This research was conducted on a model swirl combustor designed to represent swirl stabilized combustion systems such as gas turbines, or diffusion flame burners used in boilers in electrical utilities. The combustor was built to be suitable to conduct both premixed and non-premixed combustion experiments, as documented in [1,8]. In this research, only non-premixed combustion was studied.

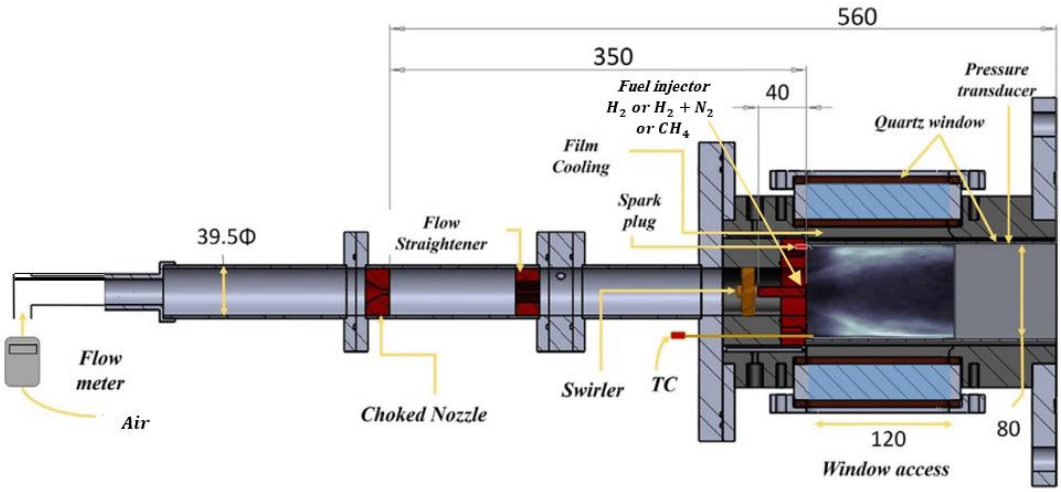

Figure 4. Schematic of swirl-stabilized non-premixed combustor (all measurements taken in mm) [8]

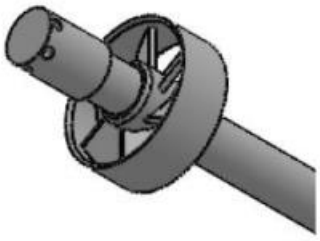

[1]

Figure 5. Fuel injector & swirler

Before the experiment, the air is contained in a reservoir with a volume of 1 m^3 which can withstand a pressure of a maximum of 200 bar. The air is diluted with nitrogen and delivered to the combustor through a 39.5 mm diameter cylindrical tube, goes through a choked nozzle meant to lessen fluctuations in equivalence ratio caused by acoustics disturbances, and later through a flow straightener to reduce turbulence intensity, until it meets the swirler and expands into the square-shaped combustion chamber (80 x 80 x 210 mm). Finally, the flow exists from the combustor to the atmosphere in an open end. Four

quartz windows of 30 mm thickness are providing a 120 x 80 mm viewing area. In previous experiments, the data regarding pollutant emissions of NO_x was collected using a 3 mm alumina tube placed on top of the combustor and cooled by water. The swirler consists of six vanes located at $60°$ from one another, and the fuel is injected through the center of the swirler using a separate body with 6 fuel injection ports, each has a 3 mm diameter, located 5 mm from the dump plane. The swirl number is defined as the ratio of angular momentum's axial flow rate to linear momentum flow rate [4]. Kozo Aoki et al. [9]:

$$S = \frac{\int_{R_{\text{in}}}^{R_{\text{out}}} u_\theta u_z r^2 dr}{(R_{\text{out}} - R_{\text{in}}) \int_{R_{\text{in}}}^{R_{\text{out}}} u_z^2 r dr} \tag{7}$$

The importance of the swirl number is it can help understand the structure of the swirling flow, the formation of inner recirculation regions, or of PVC- precessing vortex core (which involves swirling flows undergoing vortex breakdown) [10].

We will use the mean swirl number as it is represented by N. Balasubramanian et al. [8] in the following equation:

$$S = \frac{2\left(1-\left(\frac{D_h}{D_{in}}\right)^3\right)}{3\left(1-\left(\frac{D_h}{D_{in}}\right)^2\right)} \tan\theta \tag{8}$$

D_h- diameter of the hub, equals 39.5 mm, D_{in}- effective diameter of the inlet, equals 80 mm,

θ- vane angle, equals $60°$.

The swirl number in this swirler setup is 1.

Measurements Technique

The high speed and complexity of combustion processes raise the need for sufficient measurement techniques. In this research, we used planar laser-induced fluorescence (PLIF).

Planar Laser-Induced Fluorescence

The mechanism

The flow entering the combustor is exposed to a planar laser light. Chemical species are excited by the laser, causing fluorescence to occur. The fluorescence emission is then captured on a digital camera. Fluorescence is the emission of light by a substance that has absorbed light or other electromagnetic radiation. The incoming photons increase the energy of electrons in the molecule to an excited state. These electrons then lose a bit of energy in the form of heat due to vibrations of the molecules, and eventually, they return to the ground state by releasing photons. Meaning the energy of light emitted is slightly lower than the energy of the light that is absorbed.

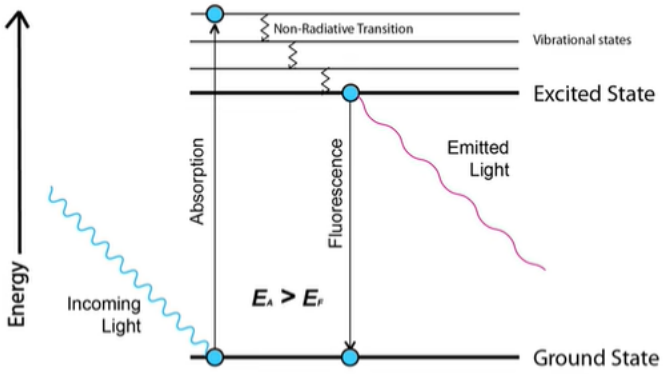

[11]

Figure 6. Fluorescence emission representation

When using an ultraviolet laser, that has higher energy than the visible region, the invisible ultraviolet photons absorbed can stimulate the emission of photons in the visible region.

This way PLIF allows us to observe specific species participating in the combustion, and capture cross-sectional information. The laser system's frequency is 10 Hz, meaning the PLIF camera captures only 10 frames per second. For comparison, a chemiluminescence camera can capture up to 4,000 frames per second. The evolution of the flame is too quick to capture due to the limitations in imaging frequency when using PLIF, however, further calculations of statistics such as the flame's location and surface area are needed to learn the spatial evolution of the flame. Each laser pulse has an energy of approximately $30\ mJ$ and lasts $5\text{-}6\ ns$, providing an instantaneous location of the flame. In addition, smoothing filters

were applied to address any noise. The laser was turned to produce an ultraviolet beam at the wavelength of approximately 283 nm to perform OH PLIF. By analyzing and comparing the data gathered we gained a better understanding of the characteristics of the flames, reaction zone, and fuel/air mixing nature.

The optical setup

The system of PLIF consists of a Nd: YAG laser (TRLiG 850-10), a UV tunable dye laser (LiopStar-E), and a CMOS camera (Andor Zyla 5.5), See Fig. 4.

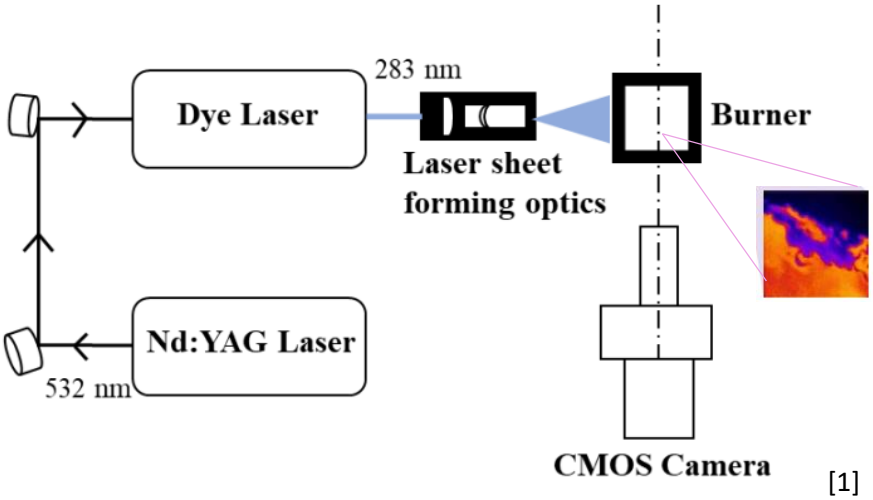

[1]

Figure 7. OH-PLIF system schematic

As stated before, fluorescence is induced by the sheet of laser light, and later captured by the CMOS camera. The sheet of laser light is formed with Nd:YAG laser (neodymium-doped yttrium aluminum garnet), which uses a crystal of YAG (solid) doped with neodymium ions to emit a high-intensity laser beam in the infrared region. The UV dye laser uses an organic dye as the lasing medium, in comparison to the YAG crystal in the Nd:Yag laser. The dye is pumped by the Nd:Yag laser – it absorbs the light energy, and then emits the energy in the form of an ultraviolet beam laser light at a tunable wavelength. To excite OH molecules a Rhodamine 590 dye was used to produce a laser beam with a wavelength of 282.93 nm.

The laser beam then passes through light sheet optics that control its size and shape to expand it to a planar form. The resulting laser sheet is directed with mirrors into the combustor, aligned with its centerline. After it excites the OH molecules and fluorescence is emitted, the fluorescence meets UV lens (Nikon 105 mm, f/4.5) mounted with an OH bandpass filter (310 ± 10 nm), until it reaches the intensified CMOS camera, with the intensifier gate opening 70 ns after the trigger from the laser for a duration of

190 ns. The size of the captured image is 2160 x 2560 pixels, out of which 1410 x 1710 is equivalent to 82 x 100 mm viewing area, meaning a spatial resolution of 0.058 mm.

Computational Methods

One-Dimensional Flame Analysis

The calculations were made using the GRI- Mech 3.0, the 53-species, 325-reaction natural gas combustion mechanism developed by Gregory P. Smith et al. [12] This mechanism was implemented to simulate non-premixed one-dimensional flames.

The function CounterFlowDiffusionFlame simulates an opposed flow created by two inlets, one of fuel (hydrogen or methane or hydrogen diluted by nitrogen) and the other of oxidizer (air), fitting to the four cases listed earlier. The conditions of each inlet were set to 1 atm pressure and 300 K temperature.

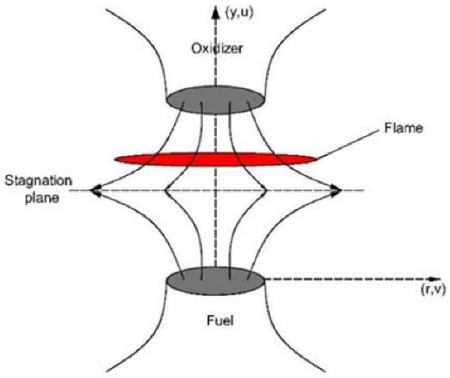

[13]

Figure 8. An opposed flow non-premixed flame

According to the laminar flamelet concept, a structure composed of basic laminar diffusion flames can represent a turbulent diffusion flame as an entirety. N. Peter [14] reviewed the counterflow geometry as the best way of representation to study laminar flamelets, as the scalar structure of both steady laminar counterflow diffusion flame and unsteady turbulent mixing layers, is very similar. This concept is valid when observing either a “perturbed flamelet” or a “wrinkled and stretched flamelet”.

Results

As the laser beam is absorbed by the chemical species in the combustor, it slightly decreases its intensity. Therefore, in all our images the right side of the picture is brighter and more intense than the left side. All the images are approximately in the size of the viewing area, which is 120 x 80 mm.

Hydrogen/Air

Fig. 10 presents three OH PLIF instantaneous images of hydrogen/air non-premixed combustion. Fig. 11 presents an average and standard deviation over a hundred images.

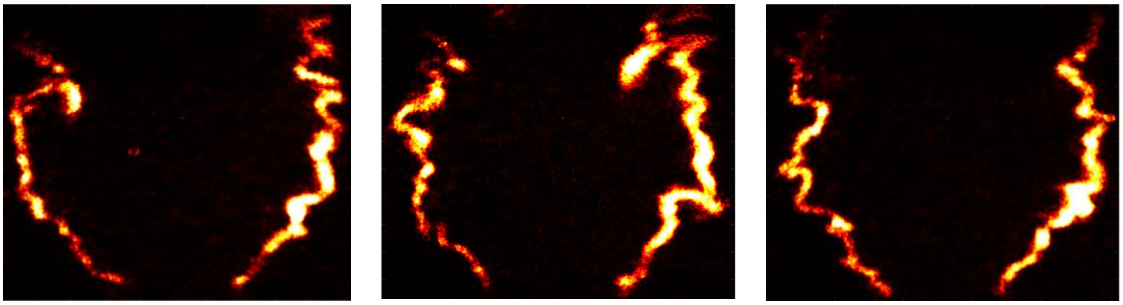

Figure 9. Hydrogen/Air OH PLIF instantaneous images

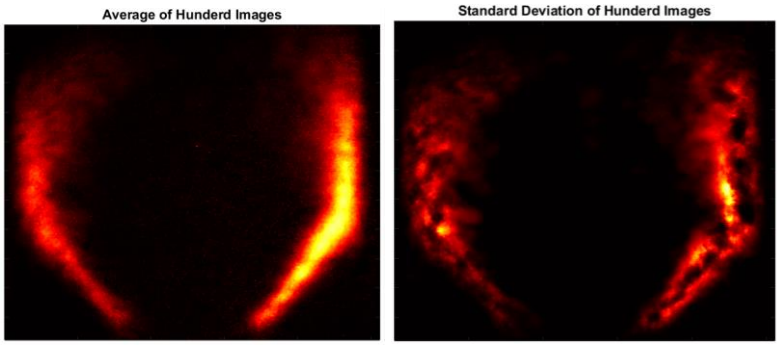

Figure 10. Average and Standard Deviation of Images

We can see the stretched flamelets at the areas where the OH concentration and the flame itself narrow. The thinning is caused by the increase in strain rates, the larger strains the flame is facing, the thinner it will become. We see it very clearly in the first three instantaneous images. Despite the laser intensity's weakening mentioned above, the average of all images shows the symmetry of combustion.

Hydrogen Diluted by Nitrogen /Air

Fig 11-15 presents non-premixed combustion of hydrogen diluted by nitrogen/ air. Fig. 11, 14 presents three OH PLIF instantaneous images while Fig. 12, 15 presents an average and standard deviation over a hundred images.

24% Nitrogen Dilution

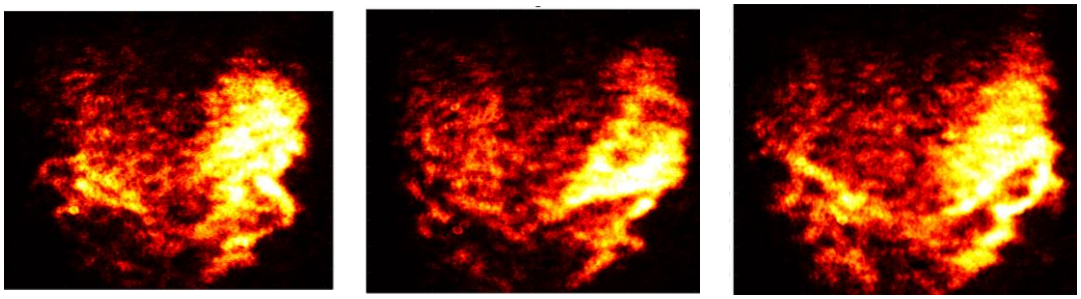

Figure 11. Hydrogen diluted by nitrogen/Air OH PLIF instantaneous images

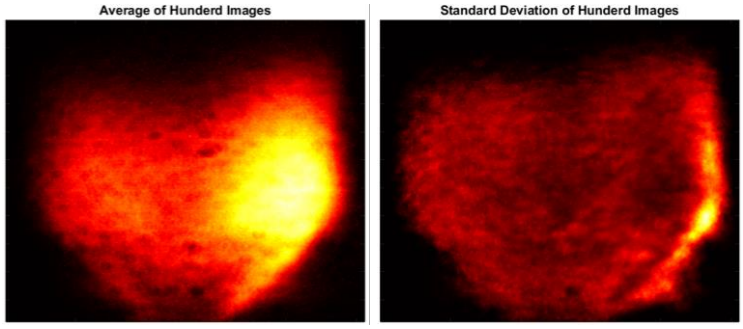

Figure 12. Average and Standard Deviation of Images

These results are different than expected. We would expect to observe OH as a thin layer representing the flame at the wrinkled and stretched flamelets regime, which is indeed the case with hydrogen/air combustion. However, when we began diluting the air with nitrogen, we can see the flame is not concentrated but in a distributed and decentralized form, and seems more similar to the form of a premixed flame, as presented in Fig.15. We can still observe there is a clear flame front, implying the flame is not yet entirely in the thickened flame regime, but is somewhere along the transition between perturbed flamelets and the thickened flame regimes.

36% Nitrogen Dilution

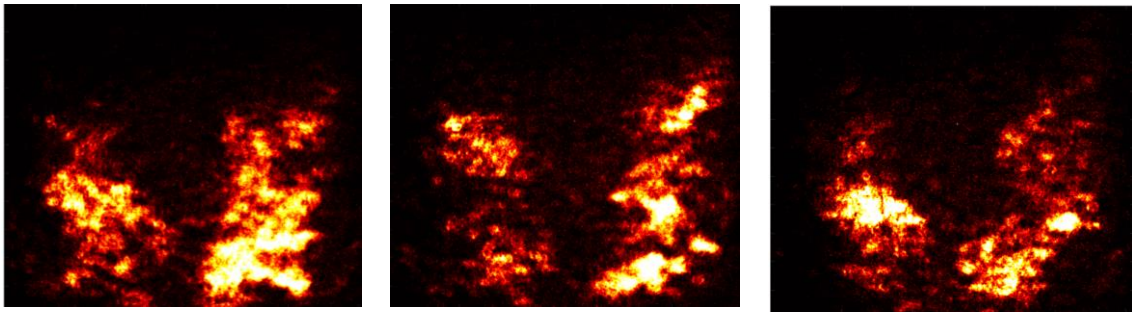

Figure 13 Hydrogen diluted by nitrogen/Air OH PLIF instantaneous images

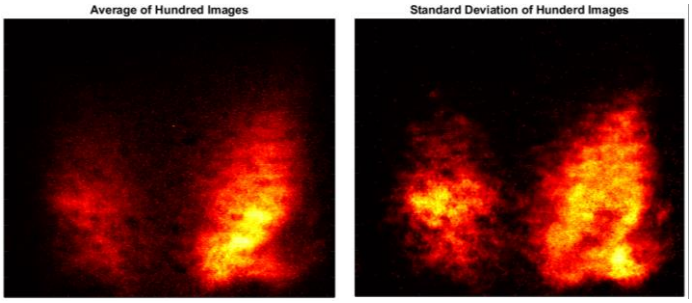

Figure 14. Average and Standard Deviation of Images

With 36% nitrogen dilution there is no clear flame front, Da is low and quenching begins, the flame is now very similar to the form of a premixed flame [1] and can be classified as a thickened flame. In addition, the OH concentration begins to seem a bit thinner again, more focused, than with 24% nitrogen dilution. We suspect the cause is the augmented momentum of the nitrogen, that enhances fuel/air mixing. Higher dilution might hold a greater effect on the chemical reaction than it does on the flow's momentum. According to Eq. 7 $D_a = \frac{|l_f|^2}{D_f \cdot \tau_c}$. An increase in the chemical rate τ_c will lower Da to the thickened flame regime and begin local quenching (Fig.3). The images received resemble ones of a premixed flame. For example, a premixed hydrogen/air flame:

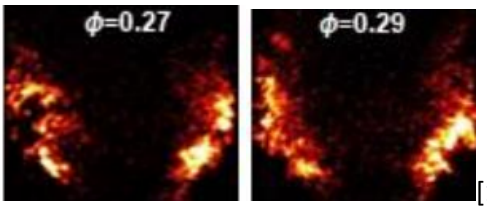

[1]

Figure 15. OH PLIF instantaneous images of premixed hydrogen/ air combustion at $\phi = 0.27, 0.29$

Methane/Air

Fig. 16 presents three OH PLIF instantaneous images of methane/air non-premixed combustion. Fig. 17 presents an average and standard deviation over a hundred images.

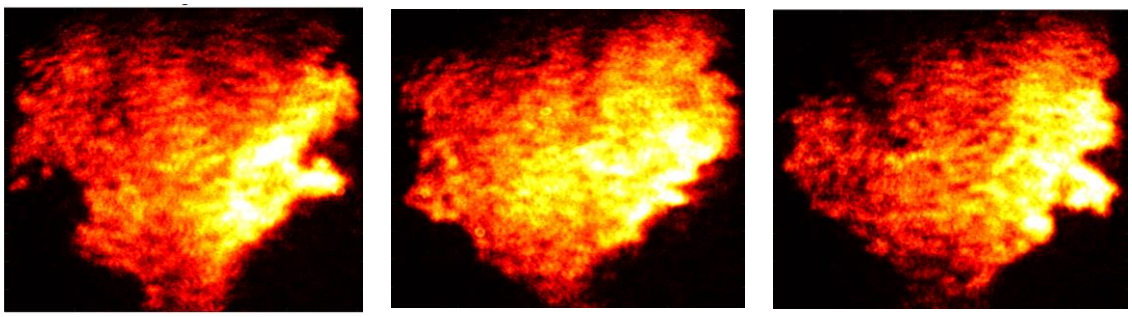

Figure 16. Methane/Air OH PLIF instantaneous images

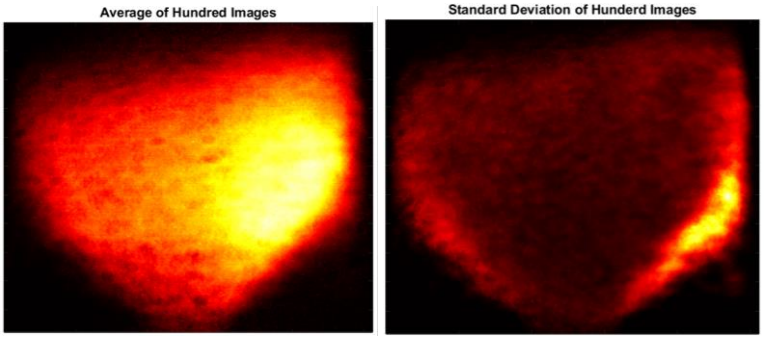

Figure 17. Average and Standard Deviation of Images

These results match our assumptions, as OH is known to remain a product of methane/air combustion. Meaning, in this case, OH will not be considered as an indication of the flame alone but as an observation of both the combustion and the product behavior.

Cantera calculations

The following simulations were made in conditions of initial room temperature (300 K) for both the fuel and oxidizer, the mass flux of the oxidizer inlet was set to 0.6 $\frac{kg}{s^2m^2}$, and the mass flux of the fuel inlet was set to 0.4 $\frac{kg}{s^2m^2}$, and the distance between the fuel and air inlets was set to be 2 cm. Let us define the chemical time rate τ_c as the inverse extinction rate.

Fig. 18-19 present each case in a range of strain rates:

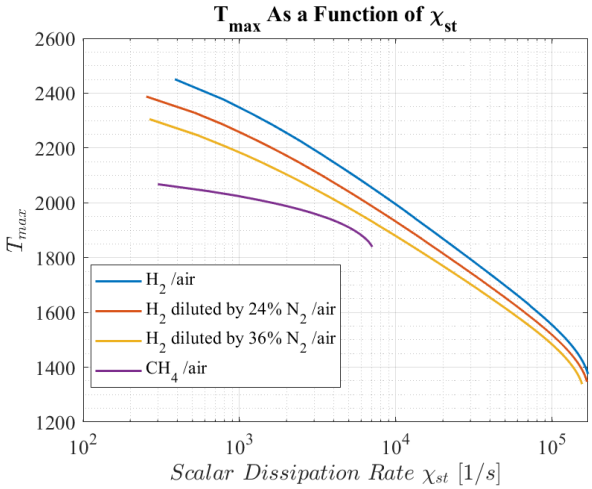

Figure 18. Maximum Temperature as a Function of Scalar Dissipation Rate

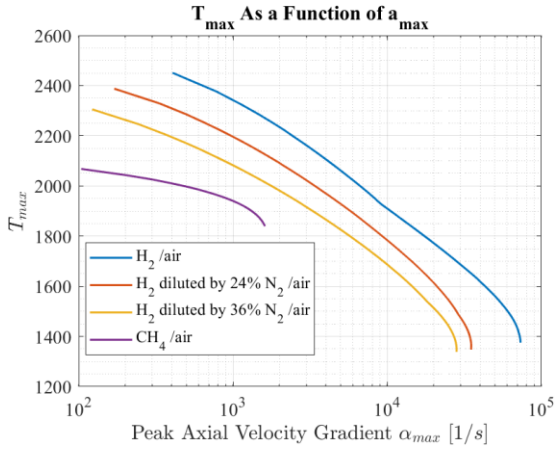

Figure 19. Maximum Temperature as A Function of the Maximum Axial Velocity Gradient

Fig. 18 and 19 both show the way peak temperature in each case is affected by different strain rates until the flame is extinguished. The extinction point of the flames was computed using Cantera's simulation of a counterflow diffusion flame and the scaling rules derived by Fiala and Sattelmayer [7].

The maximum temperature received for a peak axial velocity gradient of zero should be equal to the adiabatic flame temperature:

	HYDROGEN	HYDROGEN DILUTED BY 24% NITROGEN	HYDROGEN DILUTED BY 36% NITROGEN	METHANE
ADIABATIC FLAME TEMPERATURE	2,380 K	2,264 K	2,173 K	2,225 K

Table 1. Adiabatic flame temperature for a stoichiometric mixture.

These values indicate a decrease in maximum temperature is expected in lower flame strain rates, although it is not yet seen in Fig. 20. By the course of the plots shown in Fig. 20 we would expect the temperature to be higher in lower strain rates for cases 1-3, and lower for case 4.

With the addition of nitrogen, following our expectations, the peak temperature decreases. As mentioned earlier, nitrogen dilution causes the reduction of NO_x emissions by lowering the combustion temperature. The calculations are made for flames in the wrinkled and stretched flamelets regime. The effects nitrogen addition holds on combustion are in both the turbulent flow and the chemical reaction. While the change in turbulent flow is partially shown in Fig. 18 and 19 above, the chemical effects are shown in Fig. 10-15- the PLIF images. We concluded the flames are transitioning in different cases to different regimes, from wrinkles and stretched flamelets to perturbed flamelets and even to thickened flame, which resembles a premixed flame. Further investigation is required to validate these assumptions, however, if the flame becomes partially premixed due to nitrogen dilution, its peak temperature will decline even further. In each simulation from the four listed above, the maximum temperature declines

As turbulent flow becomes more dominant, flame thickness decreases and scalar dissipation rate increases, leading to a decrease in maximum flame temperature in all cases, until extinction.

Fig. 21 presents the peak molar fractions of OH, NO and NO_2 for flames in a range of strain rates:

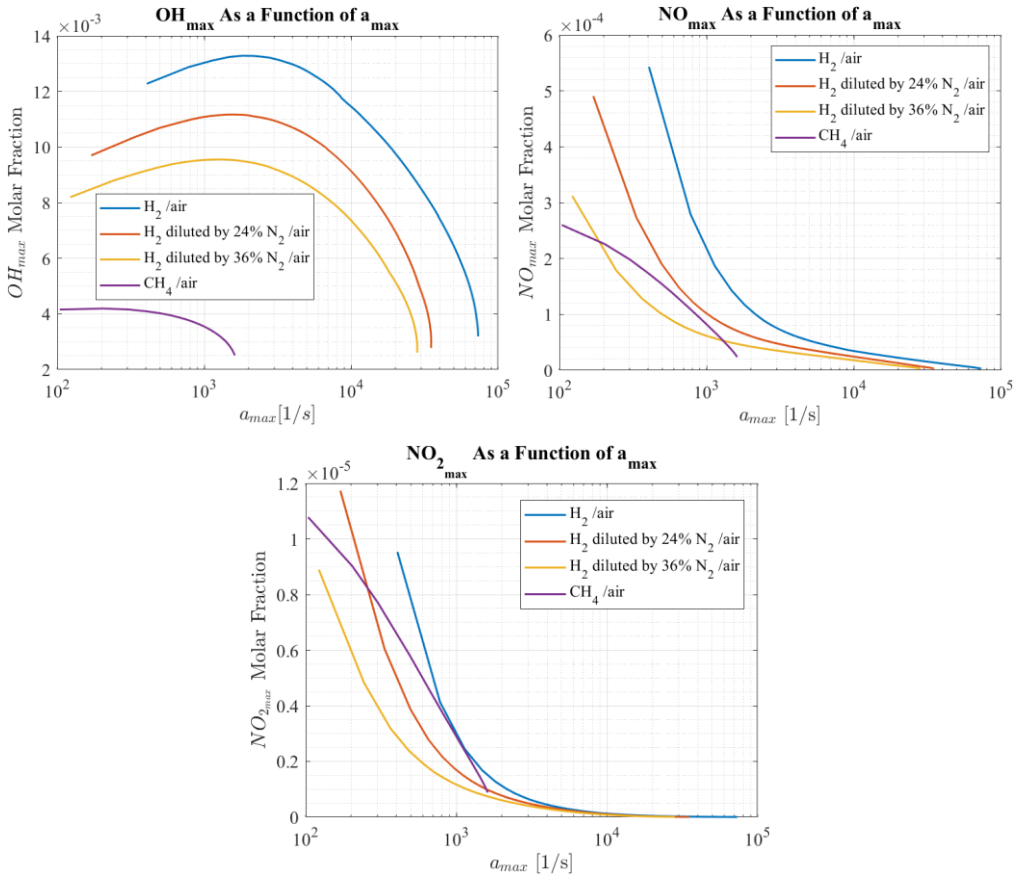

Figure 20. Maximum Molar Fractions of OH, NO, and NO_2 at different flame strain rates, as a function of peak velocity gradient.

Each of the four cases were investigated in different global strain rates, kept at equal fuel and air fluxes:

Case 1: Hydrogen/ air, global stretch rate of $\frac{\Delta V}{z}$ =153.4 [1/s].

Case 2: 24% Nitrogen-diluted Hydrogen/ air, global stretch rate of 34.6 [1/s].

Case 3: 36% Nitrogen-diluted Hydrogen/ air, global stretch rate of 17.9 [1/s].

Case 4: Methane/ air, global stretch rate of 5.2 [1/s].

Data from the four cases studied is presented in Table 2:

	OH peak molar fraction	NO peak molar fraction	NO_2 peak molar fraction	Maximum temperature
Hydrogen/Air	$1.3 \cdot 10^{-2}$	$2 \cdot 10^{-4}$	$2.8 \cdot 10^{-6}$	2,341 K
	At 2284 K	at 2311 K	at 643 K	
Hydrogen diluted by 24% nitrogen/ air	$1.06 \cdot 10^{-2}$	$1.6 \cdot 10^{-4}$	$3.2 \cdot 10^{-6}$	2,266 K
	At 2228	at 2257 K	at 691 K	
Hydrogen diluted by 36% nitrogen/ air	$0.9 \cdot 10^{-2}$	$1.1 \cdot 10^{-4}$	$2.7 \cdot 10^{-6}$	2,185 K
	At 2167 K	at 2182 K	at 747 K	
Methane/ air	$4 \cdot 10^{-3}$	$2 \cdot 10^{-4}$	$7 \cdot 10^{-6}$	2,018 K
	at 1882 K	at 1978 K	at 673 K	

Table 2. Data from an Investigation of Four Cases

With the addition of nitrogen, we see a reduction both in the peak OH molar fraction and peak NO molar fraction, as expected. OH concentration is indeed known to decrease with decreasing temperature, and NO pollutant emissions are known to decline with dilution by nitrogen.

The NO_2 peak molar fraction increases with nitrogen dilution at first, until it decreases with 36% nitrogen dilution. The quantities of NO_2 pollutant emissions are two orders of magnitude less than NO, making it even negligible in the process. The rise in NO_2 emissions between the case with no dilution and 24% dilution can be assumedly due to the temperature rise those peaks are accepted in, or the distributed form of the flame. The reduction between the case with 24% dilution and 36% dilution is expected and is probably due to the lower maximal temperature of the experiment caused by nitrogen addition, as well as the subtle thinning of the flame.

In methane/air combustion, the peak OH molar fraction is one order of magnitude smaller than in all previous cases, due to lower combustion temperature (about 200 ~ 300 degrees less than the other

experiments). NO_2 emissions, on the other hand, are higher than in the other cases despite the lower flame temperature.

Each case will be presented separately in Fig. 22-25:

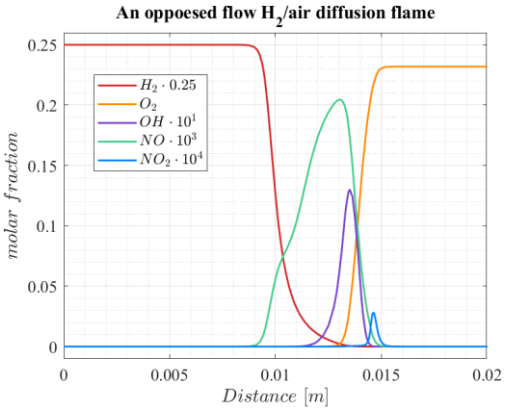

Figure 21. Molar Fractions of Reactants, OH, NO, and NO_2 VS. distance, Case 1

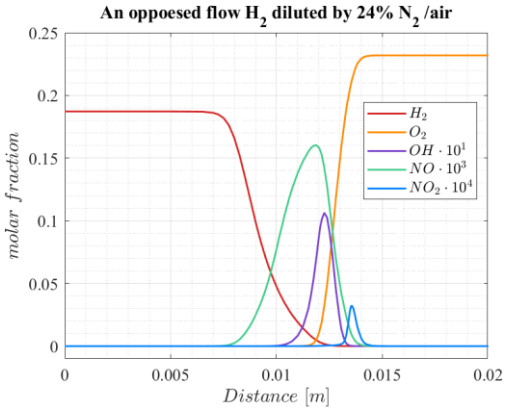

Figure 22. Molar Fractions of Reactants, OH, NO, and NO_2 VS. distance, Case 2

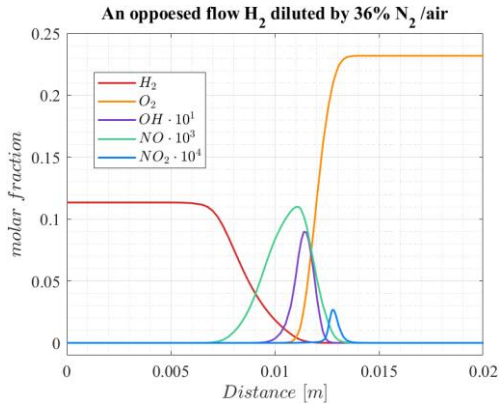

Figure 23. Molar Fractions of Reactants, OH, NO, and NO_2 VS. distance, Case 3

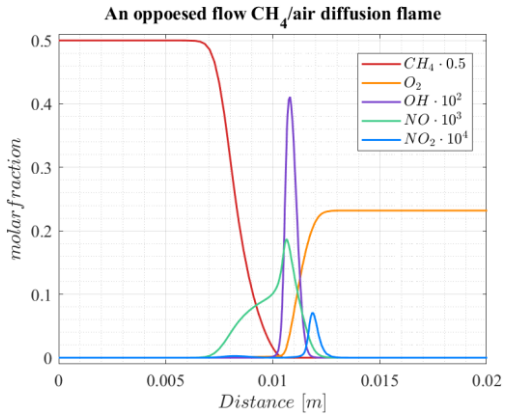

Figure 24. Molar Fractions of Reactants, OH, NO, and NO_2 VS. distance, Case 4

The cases in the experiments were tested with larger strain rates than in the simulations. Based on Fig. 18-20, the actual peak temperature will be lower, leading to reduced pollutant emissions than presented in Fig. 21-24.

Conclusions

The experimental results we received mainly fit our expectations before the experiments, with few exceptions. OH PLIF images captured for hydrogen/air combustion showed a rather symmetric, thin-layered turbulent flame front. Images from nitrogen-diluted hydrogen experiments showed OH was not concentrated in a thin layer but in a more distributed and decentralized form, where the flame front is broken; suggesting it can be classified in either the thickened flame regime or in some sort of transition between the perturbed flamelets and thickened flame regime. A possible explanation for the transition could be a higher Re number in the injector the nitrogen addition provided, and its effect on the chemical reaction. The transition to perturbed flamelets and later thickened flame implies the decrease in Da value, according to Fig. 3. We defined in Eq. 6 $D_a = \frac{\tau_f}{\tau_c}$ meaning τ_c is increased due to dilution (flame extinction time is decreased, as its inverse), and τ_f decreased due to the higher Re number in the injectors. If we consider the flame as partially premixed, we can discuss the raise in Ka value, being the inverse of Da. Let us be reminded of Eq. 7,8: $Ka = \frac{\tau_f}{\tau_\eta} = \frac{l_f^2}{\eta^2} \implies For\ Ka > 1,\ l_f > \eta$. The discontinuous flame front is presumably caused by eddies becoming smaller than the reaction zone, meaning Ka was increased due to dilution.

Methane/air combustion provided results that matched our expectations, OH remains as a product of methane/ air combustion, therefore we observe in the PLIF images both the flame front, combustion zone, and the reaction products.

The simulations show that NO emissions decrease with higher nitrogen dilution, but NO_2 emissions do not consistently decline with increasing dilution, noting that its emissions are two orders of magnitude smaller compared to NO emissions. For 36% nitrogen dilution, NO emissions were lower than those in methane/air combustion, for a certain range of flame strain rates, received between peak axial velocity gradient of 204 [1/s] and 1,290 [1/s]. These results are received from one-dimensional simulations valid for wrinkled and stretched flamelets, which is not true for cases 2 and 3, therefore they provide us with a general understanding and not accurate information of neither the pollutant emissions quantities nor the three dimensional process and turbulent flow effects on the flame dynamics.

To continue the research properly, a particle image velocimetry (PIV) measurement is recommended to analyze the flow velocity from the images and to understand what strain rates exist and the interactions

of eddies with the flame. Additionally, performing acetone PLIF experiments will help in learning the fuel/air mixing behavior, and premixed or partially premixed simulations to understand the thickened flame properties and have a more complete understanding regarding diluted hydrogen combustion.

References

[1] D. Michaels, R. Kaner, P.K. Ojha, D. Cao. “Experimental and numerical investigation of combustion dynamics in a model gas turbine combustor using hydrogen and natural gas mixtures” (2023).

[2] Legrand, Jack, ed. Advances in Chemical Engineering. Edited by Jack Legrand. First edition. Amsterdam, Netherlands: Academic Press, (2016): 273-385.

[3] Borghi, R. “Turbulent Combustion Modelling.” Progress in Energy and Combustion Science 14, no. 4 (1988): 245–92.

[4] Vignat, Guillaume, Daniel Durox, and Sébastien Candel. “The Suitability of Different Swirl Number Definitions for Describing Swirl Flows: Accurate, Common and (over-) Simplified Formulations.” Progress in Energy and Combustion Science 89 (2022).

[5] Veynante, Denis, and Luc Vervisch. “Turbulent Combustion Modeling.” Progress in Energy and Combustion Science 28, no. 3 (2002): 193–266.

[6] David G. Goodwin, Harry K. Moffat, Ingmar Schoegl, Raymond L. Speth, and Bryan W. Weber. *Cantera: An object-oriented software toolkit for chemical kinetics, thermodynamics, and transport processes*. https://www.cantera.org, 2023. Version 3.0.0.

[7] Fiala, Thomas & Sattelmayer, Thomas. “Nonpremixed Counterflow Flames: Scaling Rules for Batch Simulations.” Journal of Combustion. (2014).

[8] Balasubramanian, Nikhil et al. “Mitigation of Combustion Instabilities by Local Diluent Injection in a Premixed Swirl Stabilized Combustor.” Combustion and flame 245 (2022).

[9] Aoki, Kozo, et al. "Response of heat release rate to flame straining in swirling hydrogen-air premixed flames." Flow, Turbulence, and Combustion 104 (2020).

[10] Syred, Nicholas. “A Review of Oscillation Mechanisms and the Role of the Precessing Vortex Core (PVC) in Swirl Combustion Systems.” *Progress in Energy and Combustion Science* 32, no. 2 (January 1, 2006): 93–161.

[11] Thomas, Sabu, ed. Thermal and Rheological Measurement Techniques for Nanomaterials Characterization. Edited by Sabu Thomas [and Three Others]. Amsterdam, Netherlands: Elsevier, (2017): 1-36.

[12] Gregory P. Smith, David M. Golden, Michael Frenklach, Nigel W. Moriarty, Boris Eiteneer, Mikhail Goldenberg, C. Thomas Bowman, Ronald K. Hanson, Soonho Song, William C. Gardiner, Jr., Vitali V. Lissianski, and Zhiwei Qin http://www.me.berkeley.edu/gri_mech/

[13] Chen, Y., J. Wang, X. Zhang, and C. Li. “The Effects of CO2 Additional on Flame Characteristics in the CH4/N2/O2 Counterflow Diffusion Flame.” *Molecules* 26, no. 10 (2021).

[14] Peters, Norbert. "Laminar diffusion flamelet models in non-premixed turbulent combustion." Progress in energy and combustion science 10.3 (1984): 319-339.

[15] Peters, N. “Laminar Flamelet Concepts in Turbulent Combustion.” Symposium (International) on Combustion [papers]. 21.1 (1988): 1231–1250.